DUPLICATE ALSO

162

Forecasting Research

Met O 11 Scientific Note No. 6

On the incorporation of atmospheric boundary layer effects into a balanced model

by

M.J.P. Cullen

June 1988

ORGS UKMO M

National Meteorological Library
FitzRoy Road, Exeter, Devon. EX1 3PB

Meteorological Office (Met O 11)
London Road, Bracknell, Berkshire RG12 2SZ, England

METEOROLOGICAL OFFICE
152987
14 OCT 1988
LIBRARY

MET O 11 SCIENTIFIC NOTE N° 6

ON THE INCORPORATION OF ATMOSPHERIC BOUNDARY LAYER EFFECTS INTO A BALANCED MODEL.

M.J.P. Cullen

LONDON, METEOROLOGICAL OFFICE.
Met.O.11 Scientific Note No.6

On the incorporation of atmospheric boundary layer effects into a balanced model.

04901088 551.509.313 551.510.522 551.553.11 FH2A

Met O 11 (Forecasting Research)
Meteorological Office
London Road
Bracknell
Berkshire RG12 2SZ
ENGLAND

July 1988.

N.B. This paper has not been published. Permission to quote from it must be obtained from the Assistant Director of the Forecasting Research Branch of the Meteorological Office.

ON THE INCORPORATION OF ATMOSPHERIC BOUNDARY LAYER EFFECTS INTO A BALANCED MODEL

M. J. P. Cullen

Meteorological Office, Bracknell, Berks., U. K.

SUMMARY

A method of coupling the thermal and frictional forcing in the atmospheric boundary layer to a semi-geostrophic model of the internal dynamics is developed. It is illustrated by two-dimensional sea-breeze simulations, which are compared with those of a two-dimensional primitive equation model. It is demonstrated that the main features of the circulation on a horizontal scale larger than 20 km can be simulated with the semi-geostrophic model, but the detailed local circulations cannot. It is also demonstrated that very high vertical resolution may be needed to obtain accurate simulations of the local circulations using a primitive equation model.

1. INTRODUCTION

As the resolution of numerical models of the atmosphere and the sophistication of the representation of physical processes in them increases, understanding of the interactions between explicitly represented dynamics and parametrized sub grid-scale processes becomes more important. In particular, it is necessary to ensure a correct coupling of parametrized processes with the balanced dynamics most important for weather forecasting. In this paper we study some aspects of this interaction.

The definition of balanced dynamics used here is described in a recent paper, Cullen et al. (1987b), henceforward referred to as C. This is based on an energy principle. It is equivalent to Lagrangian semi-geostrophic theory away from the equator, and reduces to an evolving static solution at the equator. It can describe a variety of flows driven by diabatic effects. Shutts (1987) has shown that several important aspects of penetrative slantwise convection are described by the model. In this paper we examine the interaction of the atmospheric boundary layer with the geostrophic dynamics in a simple sea-breeze model. Such a solution was included in C, neglecting frictional effects. It gives a reasonable estimate of the inland penetration of the sea-breeze including its dependence on latitude. Chynoweth (1987) has extended this solution to much higher resolution and included the effects of imposed gradient winds.

The interaction between semi-geostrophic theory and boundary layer structure has been studied in some detail by Wu and Blumen (1982). They assume that the geostrophic flow is independent of height within the boundary layer, and derive an Ekman solution that matches the total

semi-geostrophic flow at the boundary layer top. They considered that the main limitation of their work in explaining observed behaviour was the need to assume a constant eddy viscosity in order to obtain analytic solutions. Young (1973) also developed an approximation to the boundary layer equations which matches semi-geostrophic theory in the free atmosphere. He defines a low order solution for the velocity which satisfies geostrophic balance outside the boundary layer and Ekman balance within it, and then approximates the momentum in the full equations by its lowest order value. Neither of these solutions include the thermal forcing.

In this paper both thermal and frictional effects are considered and the assumption of constant eddy viscosity is not made. Numerical rather than analytic solutions are therefore obtained. Observed sea-breeze behaviour suggests that the thermal and frictional effects on the wind are often of the same order of magnitude. Under these conditions the Ekman solution may not be a good first approximation. The approximate equations are therefore derived directly from the two-dimensional primitive equations by neglecting the acceleration component normal to the coast. This produces a quasi-balanced sea-breeze response and gives the normal semi-geostrophic equations above the boundary layer. Yuen and Young (1986) carry out a detailed scale analysis which suggests that this approximation is reasonable if the boundary layer is deep, the capping inversion strong, and the sea-breeze itself light.

In C the semi-geostrophic equations are solved in a Lagrangian form which allows the treatment of discontinuous solutions. When this formulation is applied to real flows it should be supplemented by a parametrization of turbulent mixing and entrainment processes. In such a

formulation friction is most naturally treated as a lower boundary drag, rather than a viscosity. The thermal forcing is also imposed at the lower boundary. The effects of both can be spread in the vertical using a turbulence parametrization, which will incorporate the observed dependence of this spread on the stability and vertical shear. In this paper we use the parametrization from the U.K. Meteorological Office operational forecast model as described by Bell and Dickinson (1987).

The resulting model is applied to a simple sea-breeze simulation. Under the conditions described by Yuen and Young it should be able to describe the inland propagation of the sea-breeze. It should also be able to describe the dependence on the large scale geostrophic wind which is known to determine the occurence, strength and penetration of the front, Atkinson (1981), Houghton (1984). It cannot, however, describe the dynamics of the sea-breeze front itself, which appears to behave as a gravity current, Simpson (1969). The model should also be able to determine the qualitative balance between thermal and frictional effects at a coastline, which determines whether it is a zone of low level convergence or divergence.

The purpose of the model is to illustrate how the frictional and thermal effects of the boundary layer can be coupled directly to balanced dynamics. A two-dimensional idealised model such as this cannot give quantitative predictions of real sea-breeze effects, but can be verified against typical gross features of the circulations. Integrations with a primitive equation model using the same boundary layer parametrization and vertical and horizontal resolution are also carried out. These help to clarify how much can be expected from the model.

2. THEORETICAL DEVELOPMENT

The primitive Boussinesq hydrostatic equations for flow in an (x,z) cross-section are written using the modified pressure coordinate of Hoskins and Bretherton (1972) with boundary layer forcing terms added:

$$Du/Dt + \partial\phi/\partial x - fv = F_u \quad (1)$$

$$Dv/Dt + f(u-u_o) = F_v \quad (2)$$

$$\partial\phi/\partial z - g\theta/\theta_o = 0 \quad (3)$$

$$D\theta/Dt = H \quad (4)$$

$$\partial u/\partial x + \partial w/\partial z = 0 \quad (5)$$

$$D/Dt \equiv \partial/\partial t + u\partial/\partial x + w\partial/\partial z \quad (6)$$

$$u = u_o \text{ at } x = \pm L \quad (7)$$

$$w = 0 \text{ at } z = 0, H. \quad (8)$$

The only y variation is an assumed basic state pressure gradient in geostrophic balance with a wind component u_o which is independent of x and z. F_u, F_v and H represent the frictional and thermal forcing terms. The boundary conditions are w=0 at z=0,H; u=v=0 at z=0; and (u,v) fixed at x=±L.

Hoskins and Bretherton (1972) show, by considering a coordinate frame moving with a front, that the two-dimensionality allows Du/Dt to be neglected compared with the other terms in (1). This scale analysis may not apply for strong sea-breeze flows because the values of u relative to the front may be large and v may initially be small or zero. However, the same approximation may be valid if there is a balance between the pressure gradient and friction terms. It is also valid if the Ekman balance is valid. Yuen and Young's 'quasi-geostrophic' response to a cold air outflow is obtained if Du/Dt is neglected. Since we wish to consider both thermal and frictional boundary layer effects

the Ekman solution, which is dynamically unstable, may not be accurate. We therefore do not use the system of equations obtained by Young (1973) which use the Ekman solution as a first approximation.

In this paper we therefore neglect the term Du/Dt in (1) and make no other approximations. In particular the term Dv/Dt in (2) is not approximated. The resulting system is:

$$\partial\phi/\partial x - fv = F_u, \tag{9}$$

together with (2) to (8).

We now derive the energy equation for this system. Define the energy of a fluid parcel E as

$$E = \tfrac{1}{2}v^2 - g\theta z/\theta_0. \tag{10}$$

This obeys the equation

$$DE/Dt = uF_u + vF_v - gzH/\theta_0 - u\partial\phi/\partial x + vu_0 - w\partial\phi/\partial z. \tag{11}$$

The last three terms represent the rate of working by the pressure field. The other terms represent energy changes due to thermal and frictional effects. Friction acts as an energy sink if F_u and F_v are specified as drags, $-c_D u$ and $-c_D v$.

The behaviour of the system can be understood by first considering a linearised 'shallow water' form of the equations:

$$\partial\phi/\partial x - fv = -c_D u \tag{12}$$

$$\partial v/\partial t + f(u-u_0) = -c_D v \tag{13}$$

$$\partial\phi/\partial t + \phi_0 \partial u/\partial x = H. \tag{14}$$

Assuming variations proportional to $\exp(\lambda t+ikx)$ and if H is independent of u,v and ϕ, this system has two eigenvalues:

$$\lambda = (-A \pm \sqrt{B})/2c_D \tag{15}$$

with

$$A = c_D^2 + f^2 + k^2\phi_0$$

$$B = A^2 - 4k^2\phi_o c_D^2.$$

Both have negative real parts and zero imaginary parts representing damped non-oscillatory solutions. The eigenvectors can be written

$$(u, v, \phi) = \left(-1, \frac{f\lambda}{c_D+\lambda}, \phi_o ik\right)$$

Now consider the solution of these equations in a simple sea-breeze configuration. The basic state is a uniform geostrophic flow, and perturbations are forced by the differing frictional effects over land and sea and by heating of the lower levels over the land. The sea-breeze is an ageostrophic response to the thermal forcing. The associated vertical gradient of thermal wind and the ageostrophic flow are almost entirely confined to the boundary layer.

Consider first a frictionless flow with only thermal forcing. One of the eigensolutions disappears in this case, leaving v geostrophic with (v+fx) conserved following the motion. A simple solution is shown in C. It is represented in terms of finite elements on each of which (v+fx) and θ are constant. Elements in contact with the lower boundary over land are heated, and the heat spread evenly through the element in question. These solutions were further developed by Chynoweth (1987) to include much higher resolution. These show, for instance, the evolution of a well-mixed convective boundary layer over the land, the formation of a sea-breeze front and its propagation inland, and the formation of a much stronger front if there is a basic state offshore wind.

Now consider the converse case with no thermal forcing. The equations are slightly more general than those treated by Young (1973), in that v is not replaced by the v implied by Ekman balance in the Dv/Dt term. Though his simple analytic solution is no longer possible, the

frictional isallobaric wind that he describes should still be represented. The behaviour of the solution can be deduced from the eigenvectors and eigenvalues (15).

In the case $f \ll c_D$, which is the normal situation, the eigenvalues are approximately $-c_D$ and $-k^2\phi_o/c_D$. In the limit $f \to 0$ the eigenfunctions are respectively $(0, 1, 0)$ and $(k^2\phi_o, 0, ik\phi_o c_D)$. The first represents spin-down of the v component of the wind, the second represents spin-down of the pressure gradient. The spin-down of the pressure gradient is slower if the drag coefficient is large because less wind is needed for friction to balance the pressure gradient and the mass transfer needed to remove the pressure gradient takes longer. If f is small but $f \ll c_D$, the different spin-down rates for pressure gradient and wind lead to a geostrophic departure which is balanced by the friction term.

In the case $k^2\phi_o \ll f^2$, which requires very large horizontal scales or very small vertical scales, the eigenvalues are approximately $-(c_D^2+f^2)/c_D$ and $-k^2\phi_o c_D/(c_D^2+f^2)$. The first represents the establishment of the Ekman layer and the second the independence of the basic pressure gradient from the boundary layer wind field. Finally, if $c_D^2 \ll f^2+k^2\phi_o$, there is one very large and one very small eigenvalue. The first eigenvalue tends to infinity as c_D tends to zero, indicating that the frictionless limit is singular. Physically it represents rapid adjustment to semi-geostrophic balance. The second eigenvalue represents the evolution of the balanced solution. The presence of the large eigenvalue indicates that implicit numerical methods will be required to solve the system. These will ensure that numerical solutions for small c_D will be close to those for zero c_D. A similar difficulty in the nonlinear balance equations was pointed out by Moura (1976).

If friction is represented as a drag, and the u component is neglected compared with the v component, the geometrical finite element method illustrated in C can still be used. Holt (1987) obtained solutions with frictionally induced convergence into a frontal zone. Since discontinuous solutions may result, the friction cannot be represented as a non-linear viscosity. Both drag and heating are spread through individual elements. A separate turbulence parametrization has to be added to the method to spread the drag between elements. It is most natural to let a single element represent the boundary layer depth.

3. METHODS OF NUMERICAL SOLUTION

(a) *Equations for numerical solution*

In order to derive finite difference solutions incorporating a proper treatment of the lower boundary condition, as in forecast models, we use σ coordinates in the vertical, rather than the z coordinate that is most convenient for theoretical studies. The equations for the basic state geostrophic flow are:

$$\partial\phi_o/\partial x + C_p\sigma^\kappa\theta_o\partial\pi_o/\partial x - fv_o = 0 \qquad (16)$$

$$\partial\phi_o/\partial y + C_p\sigma^\kappa\theta_o\partial\pi_o/\partial y + fu_o = 0 \qquad (17)$$

where π_o is the basic state Exner function $(p_*/p_o)^\kappa$, p_* is the surface pressure, p_o is a reference pressure and $\kappa=R/C_p$. In the equation for the perturbed flow we assume that the surface pressure variation implied by the basic state is sufficiently small for $\partial\pi/\partial x$ to be expanded as $\partial\pi_o/\partial x + \partial\pi'/\partial x$. The equations for the perturbation from the basic state are then, using unprimed variables to represent perturbation quantities:

$$\partial\phi/\partial x + C_p\sigma^\kappa\theta\partial\pi/\partial x - fv = F_u \qquad (18)$$

$$\partial\phi/\partial\sigma = -RT/\sigma \qquad (19)$$

$$T = \theta(\sigma^\kappa\pi) \qquad (20)$$

$$Dv/Dt - fu = F_v \tag{21}$$

$$D\theta/Dt = H \tag{22}$$

$$\partial p_*/\partial t + \partial/\partial x((p_*+p_o)\bar{u}) + \bar{u}_o \partial p_*/\partial x + \bar{v}\partial p_o/\partial y = 0 \tag{23}$$

$$\partial/\partial x((p_*+p_o)(u-\bar{u})) + (u_o-\bar{u}_o)\partial p_*/\partial x + (v-\bar{v})\partial p_o/\partial y + \partial/\partial\sigma((p_*+p_o))\dot{\sigma}) = 0 \tag{24}$$

The finite difference models solve the equations in an (x,σ) cross-section at right angles to the coastline. The basic domain used for output extends 100 km on either side of the coast. In some integrations the domain is extended further to remove lateral boundary effects. The horizontal gridlength is 4km, with no temperature gridpoint actually on the coast. The geometrical model uses an (x,z) cross-section with surface pressure calculated diagnostically.

(b) *Finite difference grid and boundary layer parametrization*

In the finite difference models the temperatures and horizontal velocities are held at different levels, the 'Charney-Phillips' grid. This is necessary for satisfactory integration of the semi-geostrophic equations, Cullen (1988), and is used for both models to ensure comparability of layer depths. These models are written using σ $(=p/p_*)$ as vertical coordinate and 11 layers, with boundaries at $\sigma=($ 1, .975, .9, .79, .65, .51, .37, .27, .195, .125, .06, 0$)$. Temperatures and vertical velocities are stored at layer boundaries and winds at layer midpoints. In the geometric model the initial data is defined to give four isentropic layers of depth 1600m above two lower layers of thickness 800m. The depth of the model is fixed at 8000m.

This distribution of levels is typical of that used in operational forecast models, though many can now use more levels than this. It is

thus appropriate for a study of the interaction of boundary layer dynamics with the rest of the atmosphere. Most sea-breeze studies use very much higher vertical resolution and models which are confined to the lowest 2-4 km of the atmosphere.

The models are driven by incrementing the surface temperature with a heating function that varies sinusoidally in time. The surface exchanges are then parametrized in all the models, including the geometrical model, by the method used in the U.K. operational forecast model, Bell and Dickinson (1987). This defines fluxes:

$$F_u = -c_D|\underline{v}|u \tag{25}$$

$$F_v = -c_D|\underline{v}|v \tag{26}$$

$$F_\theta = -c_H|\theta|(\theta_1-\theta_*). \tag{27}$$

The drag and exchange coefficients are determined from the Richardson number in the bottom layer. In the geometrical model the layer thickness used in the calculation is half the depth of the bottom element. In the finite difference models the estimates of vertical gradients allow for the fact that velocities are stored half a level above the surface and temperatures a full level.

In the geometric model the fluxes are assumed to spread only through elements in contact with the ground. In the remainder of the boundary layer in the finite difference models, the fluxes take the form

$$F_x = -K_x\partial X/\partial z, \tag{28}$$

where K_x depends on the diagnosed boundary layer depth, the Richardson number, and the velocity gradient. The Richardson number is calculated at layer midpoints and tnen interpolated as necessary. The definition of the coefficients is given by Bell and Dickinson. However, to allow the scheme to be used with a long time step, the fluxes are added on using

an implicit method.

(c) *Geometric model*

In this method the atmospheric cross-section is represented by finite elements on each of which θ and (v_g+fx) are constant. The method is completely Lagrangian, and at each time step the elements are arranged to satisfy the geostrophic and hydrostatic equations. The method is described in detail by Chynoweth (1987) and is summarised in C.

The thermal forcing can easily be incorporated in this model. The length of each element in contact with land or sea surface is calculated, and the appropriate heat input is converted into a temperature increment. The momentum flux is calculated in the same way. The component in the y direction is added onto v_g. However, it is not possible to include the friction in the x direction in this method. This is because the construction of the element configuration uses values of θ and (v_g+fx) which are assumed to satisfy static and inertial stability. In the presence of friction, v_g may be large but the friction rather than the term fv may balance the pressure gradient. There is then no need for v_g to satisfy an inertial stability condition, and the construction cannot be uniquely carried out.

The results from this model are essentially exact for piecewise constant data, given the neglect of the F_u term. They therefore act as a valuable check on the finite difference results, given the absence of analytic solutions to the complete equations. The value of F_u can be diagnosed and checked against the actual differences between the finite difference and geometric results.

(d) *Finite difference model with semi-geostrophic dynamics in interior*

Equations (16) to (24) are approximated by second order centred finite differences using a staggered grid in which θ and $\dot{\sigma}$ are held at points on layer boundaries, and u and v at layer midpoints displaced a half grid length in the horizontal. The system of equations is implicit and solved by a predictor-corrector algorithm described in more detail by Cullen (1988). Equations (23), (21) and (22) are first advanced in time using values of u and $\dot{\sigma}$ from the previous timestep:

$$p_*^{*} - p_*^{t} = -\delta_x \bar{U}^{x} + \bar{u_o}^{x}\delta_x p_*^{x} = 0 \tag{29}$$

$$p_*^{x}(v^{*}-v^{t}) = -fU^{x} - (U+U_o)\delta_{2x}\bar{v}^{xt} - S\delta_\sigma \bar{v}^{\sigma xt} \tag{30}$$

$$p_*(\theta^{*}-\theta^{t}) = -(U+U_o)\delta_x \bar{\theta}^{xt} - S\delta_{2\sigma}\theta^{t}, \tag{31}$$

where

$$U = p_*^{x}u, \quad S = p_*\dot{\sigma}. \tag{32}$$

The boundary layer increments are then added to v and θ as described in (ii) above. In addition, the matrix coefficients

$$C_{ij} = \partial F_{ui}/\partial u_j, \tag{33}$$

where the suffices refer to vertical levels, are calculated. The next stage is to update U and S to time $t+\Delta t$ by enforcing (18) and (19). The equation that has to be solved for these variables is elliptic provided that the potential vorticity at time t is positive. This condition is frequently difficult to satisfy in the test problem because of the creation of a well-mixed boundary layer. It was shown in Cullen (1988) that a stable numerical solution could be obtained by:

(a) Modifying the θ field to ensure static stability.

(b) Modifying the v field to ensure inertial stability in the absence of friction. In the presence of friction the modification need only enforce the weaker condition $\partial/\partial x(v+fx)_i - C_{ii} > 0$ at level i, where C_{ii} is as defined in (33).

(c) Calculating U and S from U using a reduced version of the cross-front circulation equation which is elliptic provided only that the data are statically and inertially stable.

(d) Updating p_*, θ, and v, and iterating to convergence.

This procedure enhances numerical stability by ensuring that the corrections to U and S are usually underestimated at each iteration. Each calculation of U and S is elliptic if the data are statically and inertially stable, though the iteration may diverge if the potential vorticity is negative. No algorithm for enforcing positive potential vorticity on the fields was found which did not have unacceptable side-effects. Such an algorithm could be used instead of (a) and (b) and would probably improve the performance of the scheme.

In this model the procedure set out above is implemented by using vertical and horizontal convective adjustment schemes successively, and iterating them to ensure that both (a) and (b) are satisfied. Corrections ΔU and ΔS to U and S are written in terms of the vertical mean of ΔU and a stream-function:

$$\Delta U = \Delta \bar{U} - \partial\psi/\partial\sigma \qquad (34)$$

$$\Delta S = \partial\psi/\partial x. \qquad (35)$$

Equations (18) and (19) are then combined by eliminating ϕ and the residuals calculated using the values of π, θ and v denoted with a # in (29) to (31):

$$R_* = \delta_x\phi_* + C_p\underline{\theta}^x_*\delta_x\pi - fv_* - F_{u*} \tag{36}$$

$$R = \varkappa C_p\sigma^{\varkappa-1}\pi\delta_x\theta - C_p\sigma^\varkappa\underline{\underline{\delta}}^\sigma_\sigma\theta\delta_x\pi + f\delta_\sigma v = \delta_\sigma F_u. \tag{37}$$

The suffix * denotes surface values throughout. These residuals must be eliminated by correcting π, θ and v. The corrections are derived in terms of corrections to U and S by using (29) to (31).

$$\varkappa\delta_x p_*^{-1}\delta_x\Delta\bar{U} - f^2/p_*(\Delta\bar{U}-\delta_\sigma\psi)_* + C_{*j}(\Delta\bar{U}-\delta_\sigma\psi)_j = R_* \tag{38}$$

$$-\varkappa C_p\sigma^{\varkappa-1}\pi\delta_x(\underline{\underline{\delta}}^\sigma_\sigma\theta\delta_x\psi) + f^2\delta_\sigma(p_*^{-1}\delta_\sigma\psi) + \delta_\sigma C_{ij}(\Delta\bar{U}-\delta_\sigma\psi)_j = R \tag{39}$$

Note that after deriving these equations from (30) and (31), the cross-derivative terms $\delta_x\delta_\sigma\psi$ have been omitted to enhance the numerical stability as described above. The boundary conditions were ψ constant on upper and lower boundaries and $\partial\psi/\partial x$ and $\partial U/\partial x$ zero on lateral boundaries.

The implicit equations were solved directly by a block tridiagonal algorithm. The corrections to U and Σ are substituted back into (29) to (31) and iterated. It was found best to use the longest timestep that allowed the advection to be treated accurately and to iterate the corrections. Satisfactory results could then be obtained for the test problems. However, the need to satisfy the ellipticity conditions prevented a satisfactory solution being obtained if the friction term in the x direction was omitted and the heating included. This meant that a direct test against the geometric model was not possible. Tests of this algorithm against the geometric method in other problems have indicated that it gives satisfactory results, Cullen (1988).

(e) *Primitive equation model*

In this model equation (18) is replaced by

$$Du/Dt + \partial\phi/\partial x + C_p\sigma^{\kappa}\theta\partial\pi/\partial x - fv = F_u. \qquad (40)$$

Equations (19) to (24) are solved as before. The vertical finite differencing is the same as in the semi-geostrophic model, there are differences in the horizontal averaging to ensure numerical stability. Explicit leapfrog time integration was used, with a 6 second timestep and a weak time filter. The boundary layer parametrization was called every 15 minutes. Second order horizontal and vertical diffusion was added to the equations, with a coefficient increased towards the lateral and upper boundaries to reduce wave reflections. A convective adjustment scheme was used to remove instability in the vertical.

4. NUMERICAL RESULTS

(a) *Design of experiments*

Two types of experiment are illustrated. In the first, the surface temperature is initially the same, 290K, over land and sea and a sinusoidal heating function is switched on. This is chosen so that, if there was no heat flux away from the surface, the temperature would rise by 19°C in 12 hours. After 12 hours of heating and 12 hours of cooling a shallow stable layer is established over the land, so that the evolution on the second day is different from the first. In the second series of experiments gradient winds of 5 ms^{-1} are imposed in various directions.

(b) *Integrations with no basic state wind*

The typical observed behaviour is discussed in Atkinson (1981), and that over the water immediately offshore by Houghton (1984). It is for a sea-breeze circulation to develop which increases in horizontal scale. The fully developed extent at middle latitudes is of the order 30km offshore and 80km inland, though the inland penetration is very variable. The sea breeze propagates as a near-discontinuity in wind

speed and direction, the air in front of it is calm. The vertical extent of the sea-breeze is about 500m to 1 km, with a return circulation about twice as deep and half as strong. The sea-breeze dies away around sunset at the coast but can accelerate inland in the evening. The nocturnal land breeze is usually much shallower and weaker. There is a very large scatter of results in the different studies reviewed by Atkinson, emphasising that the real behaviour is strongly influenced by the details of the coastal topography and the airmass.

The initial distribution ot elements in the geometric model is shown in Fig.1. the elements are numbered so that trajectories can be followed. The solutions after 12 hours, when the heating of the surface stops, are shown in Fig. 2(a). At this time, however, there is still significant upward heat transfer into the atmosphere. The results from the geometric model show the development of a 'well-mixed' boundary layer over the land, and the deepening of the layer as illustrated by the distortion of the boundary above the second layer of elements. The air originally at the coastline has penetrated 31 km inland, but the strongest frontogenesis is about 15 km inland where elements originally 30 km apart have come together. The neglect of friction in the x direction means that thermal wind balance in the y directionis enforced throughout thc boundary layer. This means that the cold air is pushed well across the coast and the temperature never reaches 292K near the surface within the domain, as can be seen in Fig. 2(b). The average maximum implied sea-breeze over the 12 hours for any element interface is $1.3 ms^{-1}$. With friction coefficients over land for the bottom element of a typical value of $5 \times 10^{-4}\ s^{-1}$ calculated from the parametrization scheme, the friction term could balance a wind along the coast of about

6 ms^{-1}, which would be generated by inland penetration of air of 60km, about the maximum that occurs in the simulation. A simple calculation suggests that the degree of penetration will be reduced by about 30% by friction. The vertical extent of the circulation is restricted almost entirely to the bottom two layers of elements, 1.6 km deep.

The finite difference results using semi-geostrophic interior dynamics are shown in Fig. 2 (c), (d) and (e). The perturbation is confined to the lowest 2.5 km. The temperature contrast is confined closer to the coast with friction balancing the horizontal temperature gradient in the lowest layers. This agrees with the solution expected by modifying the geometric solution to allow for friction, and thus confirms that the finite difference solution is reasonably accurate. The wind near the coast is about 4ms^{-1} and has veered to about 135°. A clear sea-breeze front is visible 55km inland, where the wind suddenly increases from 135° 1.5 ms^{-1} to 155° 5.5 ms^{-1} 500m above the surface. The surface value is reduced by friction.

The primitive equation results are shown in Fig. 2 (f), (g) and (h). The θ field is not very different, except that the air is warmer over the land ahead of the sea-breeze front. This reflects the 'gravity current' propagation speed of the cold air in this model. The semi-geostrophic model contains implied higher propagation speeds because of the balance constraints. Waviness in the fields higher up in the atmosphere is visible. The v field also indicates reduced penetration of the cold air. The sea-breeze front is only 30km inland and more clearly marked. There also appears to be an upper level wind discontinuity in the return flow over the sea. The total wind contrast at the front is about 10ms^{-1}, with zero motion in front in agreement with observed

behaviour. The wind direction behind the front is about 115°. At the coast the wind is $7ms^{-1}$, with direction still 115°. The u field shows marked internal wave activity with vertical phase lines and wavelength about 4km. This type of behaviour is not seen in most sea-breeze simulations such as those reviewed by Atkinson (1981) because the models often only represent the lowest few kilometres of the atmosphere rather than the full depth.

These results suggest that the semi-geostrophic model can describe the basic inland penetration and veering of the sea-breeze, but smears out the front because the gravity current dynamics are not represented. There is thus some wind ahead of the front, rather than calm air, and the front itself is too far inland. The semi-geostrophic model gives a greater wind veer, nearer the typical observed value. This is because it produces a smaller cross-coastal wind component than the primitive equation model . The internal waves generated in the primitive equation model are only just resolved by the vertical grid. They were only weakly affected by increased damping at the top of the model, suggesting that wave reflection is not the main reason for their presence. Expansion of the integration domain laterally also had little effect. It is likely that much higher vertical resolution is needed to model the real internal wave response, while the resolution appears sufficient to model the semi-geostrophic response.

Figs. 3 and 4 show time sequences at 6 hour intervals of the cross-coastal wind from the two finite difference models. After 6 hours the main difference is in the horizontal scale of the response. The semi-geostrophic model forces 'instant' balance, giving significant wind 50 km either side of the coast. There is a strong convergence zone at the

coast because of the discontinuity in surface drag. In the primitive equation model the significant wind only spreads 30 km and there is no coastal convergence. After 12 hours the disparity in horizontal scale is less, The wind strength has dropped a little in the semi-geostrophic model . While c_D is large, the semi-geostrophic sea-breeze will be proportional to the unbalanced part of the pressure gradient, consistent with the observation that the sea-breeze is strongest when the temperature contrast is strongest, Atkinson (1981, p.162). It has increased a great deal in the primitive equation model because the acceleration rather than the wind itself is proportional to the unbalanced pressure gradient. The internal waves have become established.

After 18 hours, the semi-geostrophic model shows frontogenesis over the land, 80 km inland. This acceleration occurs as the frictional drag decreases and the solution has to move towards thermal wind balance. This agrees with observed behaviour.A land breeze 300m deep (the bottom model layer) has developed over the coast. The primitive equation model shows the inland front in a similar place, but stronger. The sea-breeze circulation is still blowing over the coast because it can only be removed by an adverse pressure gradient. This aspect of the simulation can be demonstrated in simple analytic models, such as those of Haurwitz (1947). The 'instant' reversal of the semi-geostrophic circulation is probably more realistic. After 24 hours, the semi-geostrophic model still has an inland front and a land-breeze at the coast. The primitive equation model has set up a land breeze, of 5 ms^{-1} rather than the 1 ms^{-1} in the semi-geostrophic model. It also occupies the lowest level.

After this diurnal cycle, the surface temperature is well below that

of the lowest model layer because the coupling is almost removed once the lowest layer becomes stable. The initial state for the second day is thus significantly different from the first. After 30 hours, heating of the air is only just beginning. The semi-geostrophic model has essentially no wind, indicating no forcing, and the primitive equation model has maintained its land breeze. After 36 hours, both have developed a sea-breeze, but almost entirely over the land. Both are weaker than on the first day.

These sequences indicate the fundamental difference between the models. One diagnoses the circulation from the forcing and the pressure gradient, and the other accelerates it. These idealised results suggest that both have merit at different stages of the diurnal cycle.

(c) *Results with different basic state winds*

Houghton (1984) classifies the effect of a basic state wind on the sea-breeze over the sea in terms of whether there is an offshore or onshore component of wind to add to the return circulation and whether there is coastal convergence or divergence. The picture over land, as found in the various studies referred to by Atkinson (1981), is more complicated. Houghton states that an onshore wind prevents the sea-breeze by impeding the return flow. However the thermal effect may accelerate the wind close to the coast and it is difficult to distinguish the result from a sea-breeze. The reduction in speed and change in direction over the land determines whether the coast is a zone of convergence or divergence. This zone may be displaced from the coast by the gradient wind. The sea-breeze convergence and divergence zones have to fit in with these, resulting sometimes in a displacement of the circulation away from the coast.

The basic state gradient winds used were 5 ms^{-1} in directions 225°, 340°, 160°, and 045°. These are chosen to give the four combinations of coastal convergence or divergence and offshore or onshore winds. This corresponds to the classification used in Houghton's book.

The results after 12 hours for a 225° wind and the same heating rate as used in the previous experiments are shown in Fig. 5. The layout of the results is the same as in Fig. 2. This wind direction gives a divergence zone at the coast, which will be displaced offshore. This is consistent with the sea-breeze circulation, so the frictional effect from the basic state will reinforce the thermal effect. Observations show that this is the best situation for sea-breezes, with a strong front developing near the coast. Initially the sea-breeze is normal to the coast but veers to about 160° by the end of the day. The calm zone between the sea-breeze and the gradient wind over the sea moves steadily out to sea. The sea-breeze over the land is reduced or prevented. The results from the geometrical model, Fig. 5(a), are obtained by moving the coastline relative to the elements. The width of the cross-section is 200 km. The initial position of the coast is 18 km from the right hand side of the cross-section and the final position 32 km from the left, as indicated in the diagram. The results show stronger frontogenesis than without the basic state wind. Element 60 in the centre is displaced 12 km further than in Fig.2, though the front is now out to sea. There have also been more element interchanges, with element 78 now to the left of elements 65 and 71. The front is a wind shift line, with little temperature contrast. The cooler sea air again penetrates well inland, Fig. 5(b) shows that the surface air temperature is only 291.5° 30 km inland.

Results for the semi-geostrophic finite difference model are shown in Figs. 5 (c) to (e). The cross-section is centred on the coast. The cold air has been confined to the sea, with a well-mixed boundary layer over land extending to within 10 km of the coast and surface air temperatures greater than 293°. Friction is crucial in allowing this strong thermal gradient close to the coast to be maintained in a balanced solution. The sea-breeze front is about 5 km inland. The wind shifts from 185°, 3 ms^{-1}, to 170°, 8 ms^{-1}. The return circulation results in a veering of the wind to 240° 1.5 km above the surface out to sea. There is no surface calm zone out to sea, but a gradual change towards the basic wind direction. The stronger front agrees with the geometric model and the observed behaviour. The breeze is only a little stronger than without the basic state wind. The frontal positions in the geometric and finite difference models are different because of the effect of friction.

The primitive equation results are shown in Fig. 5 (f) to (h). The effect of the basic state wind on the θ field is similar to the semi-geostrophic model. The sea-breeze reaches 13 ms^{-1} at direction 160°, about 40% stronger than with no basic state wind. The return circulation is about 3 km deep and the upward propagating wave has phase lines which tilt upstream. As in the semi-geostrophic case there is no calm zone, and the wind veers even more markedly at upper levels offshore.

These simulations all capture the observed sharpening of the sea-breeze front. Friction in the x direction is needed to capture the strong thermal gradient near the coast. Both the finite difference models reproduce some strengthening of the breeze by the basic state but neither gives the calm zone offshore.

Fig. 6 shows the results for direction 340°. This gives a coastal convergence zone which will be displaced offshore, impeding the sea-breeze circulation. The observed behaviour is for the sea-breeze to be displaced offshore with the convergence zone towards the land matching the convergence caused by the friction difference. If the same heating as in the previous experiment is used, the thermal effect swamps the frictional convergence, which is only a difference of 0.5 ms^{-1}. A reduced heating equivalent to a temperature rise of 7·5°C in 12 hours is therefore used.

In the geometric model diagrams, Figs. 6(a) and 6(b), the initial position of the coast is 18 km from the right of the section, the final position is almost in the centre. There is marked frontogenesis about 10 km offshore. The semi-geostrophic finite difference model, Figs. 6(c), (d) and (e), gives a sea-breeze of 2.5 ms^{-1} at the coast with direction 020°. Just inland the wind is backed to 270°, further inland it settles to 315°. The change in direction out to sea is more gradual. The typical observed behaviour would require a wind of 160° over the sea, with the convergence zone displaced out from the coastline. The results in this case are, however, extremely sensitive to the heating rate. With the heating rate used in Figs. 2 and 5, a wind of more than 10ms^{-1} was generated at the coast which completely swamped the efffect of the frictional convergence. The primitive equation model results, Figs. 6(f), (g) and (h), show much less internal wave generation than the previous cases, presumably because of the reduced forcing. A sea-breeze of 6 ms^{-1} in direction 080° develops with a maximum value 10 km inland. There is a strong sea-breeze front. This direction is much closer to that described by Houghton but the displacement of the sea-breeze

circulation out to sea is not modelled.

Fig 7 shows the results for direction 160°. In this case the coast is a zone of divergence, which will be displaced inland. This again impedes the sea-breeze circulation. In order to demonstrate the effect, the smaller heating rate used in Fig. 6 is employed. The observed behaviour is that the true sea-breeze overturning circulation is prevented, but that the thermal effect strengthens the onshore component of the wind. This tends to cancel out the speed reduction which would otherwise occur due to coastal divergence. Most studies reviewed by Atkinson suggest that the sea-breeze front is weakened or prevented.

In the geometric results, Figs. 7(a) and (b), the coast is initially 18 km from the left of the section, and after 12 hours is near the centre. All the element rearrangement occurs over the land. There has been a considerable overturning of the elements, in particular note the final position of elements 35 and 54. This displacement fits in with the coastal divergence zone, the corresponding effect for wind direction 340° was not captured in the results shown in Fig. 6. The lack of frontogenesis is striking. In the semi-geostrophic model, Figs. 7(c), (d) and (e), the wind offshore is increased to 6.5 ms^{-1} with little change in direction. The overturning part of the circulation is displaced over the land, as in the geometric model. The inland overturning is even more marked in the primitive equation model, Figs. 7(f), (g) and (h). The response offshore is for increased wind of 7 ms^{-1}, but the direction veers to 170°. Since this wind is upgradient, it must indicate an unbalanced inertial response.

Fig. 8 shows the results for direction 045°.The coast is now a convergence zone, which is displaced inland, helping the sea-breeze

circulation. However, the onshore component of the basic state wind impedes the return circulation and the development of the temperature contrast. The larger heating rate used in Figs. 2 and 5 is employed.

In the geometric model results, Fig. 8(a) and (b), the initial position of the coast is 18 km from the left of the section and the final position 32 km from the right. There is more of a circulation than in Fig. 7, but little frontogenesis. The semi-geostrophic finite difference model, Figs. 8(c), (d) and (e), shows an enhanced onshore wind of 6ms^{-1} at the coast. This seems incorrect in this case, and a simlar 'bulls-eye' is visible in the earlier cases very close to the coast. It appears to result from the imposition of exact balance between gridpoints only 4 km apart across a discontinuity in forcing. It does not happen in the geometric model where elements are continuously moved through the discontinuity. The rest of the solution shows a strong overturning circulation inland. This veers the wind to 090° up to 50 km inland, overcoming the frictional backing. The primitive equation model, Figs. 8(f), (g) and (h), shows a strong front 30 km inland with calm air at the surface in front of it and a wind of 090°, 9 ms^{-1} behind it. Over the sea the wind is little disturbed and gradually reaches a value of 040° 4 ms^{-1}.

Overall these experiments show that the effect of the basic state wind on the strength of the sea-breeze front, and on the sea-breeze velocity, can be reasonably captured by the semi-geostrophic model. However, the displacement of the circulation and of the coastal convergence or divergence in the direction normal to the coast do not seem to be reliably captured. These require the inclusion of the advection of the ageostrophic circulation by the basic state wind. The

primitive equation model does not capture much more useful detail. Although the extra advective effects are present, and the circulations can now be displaced from the coast, there is a large unbalanced component to the response which cannot be modelled accurately with a model of this resolution.

5. THREE-DIMENSIONAL MODEL

Though only two-dimensional calculations are performed in this paper, it is important to consider what formulation should be used in three-dimensions. Hoskins (1975) derived the three-dimensional semi-geostrophic equations by seeking a system which would reduce to his original two-dimensional form in appropriate axes if the pressure gradient was in one direction only. The equations are only valid if the flow is approximately two-dimensional so that the trajectories are nearly straight. Applying the same philosophy in the presence of friction gives the equations:

$$\partial\phi/\partial x - fv_0 = F_{u1} \tag{41}$$

$$\partial\phi/\partial y + fu_0 = F_{v1} \tag{42}$$

$$Du_0/Dt + \partial\phi/\partial x - fv_1 = F_{u0} \tag{43}$$

$$Dv_0/Dt + \partial\phi/\partial y + fu_1 = F_{v0} \tag{44}$$

$$\partial u_1/\partial x + \partial v_1/\partial y + \partial w/\partial z = 0 \tag{45}$$

$$D/Dt \equiv \partial/\partial t + u_1\partial/\partial x + v_1\partial/\partial y + w\partial/\partial z \tag{46}$$

together with (3) and (4). The suffix zero represents a first approximation to $\underline{u}$, playing the role of the geostrophic wind in the frictionless case, and the suffix 1 represents a more accurate approximation. This system is not simply that which would be obtained by using the Ekman velocity instead of the geostrophic wind in the geostrophic momentum approximation. The reason can be seen by

considering the energy equation. Representing the friction terms by drags $-c_D u$, $-c_D v$, as in (12) and (13), we have:

$$E = \tfrac{1}{2}(u_o^2+v_o^2) - g\theta z/\theta_o \qquad (47)$$

$$DE/Dt = u_o(-c_D u_o+fv_1-\partial\phi/\partial x) + v_o(-c_D v_o-fu_1-\partial\phi/\partial y)$$
$$-w\partial\phi/\partial z \qquad (48)$$

$$= -\underline{u}_1.\nabla\phi - c_D(u_o^2-u_o u_1+u_1^2+v_o^2-v_o v_1+v_1^2) \qquad (49)$$

The first term represents the rate of working by the pressure field and the second is negative definite, representing the frictional dissipation. If $\underline{u}_o$ were the Ekman velocity and the equations constructed similarly to the geostrophic momentum approximation then the suffices 0 and 1 on the friction terms in equations (41) to (44) would have to be interchanged. The energy equation (49) then reduces to

$$DE/Dt = -\underline{u}_1.\nabla\phi + c_D((u_o-u_1)^2+(v_o-v_1)^2-u_1^2-v_1^2) \qquad (50)$$

This could give positive energy changes due to friction if $\underline{u}_1$ is small and $\underline{u}_o$ is larger. Though the approximation is not accurate in such cases anyway, the possibility of energy generation makes it unsuitable for time-dependent calculations.

6. DISCUSSION

The main purpose of the paper was to demonstrate how to couple boundary layer processes to semi-geostrophic internal dynamics. This has been achieved and demonstrated in two dimensions, and a method described for three dimensions. The results of the experiments demonstrate that the gross features of the sea-breeze and its dependence on the basic state gradient wind can be described. In particular, the fact that the wind veer is caused by conservation of (v+fx) as parcels are swept inland is clearly demonstrated; it does not require parcels to be in the circulation for any fixed length of time.

The detailed results indicate the limitations of both this balanced theory and of the integration schemes used for both the balanced and primitive equation models. The balance requirement causes the initial scale of the response to be too large and the front to be smeared. The primitive equation model reproduces both these aspects well, in common with other published modelling studies. The imposition of balance allows the sea-breeze to be stopped and the land breeze set up at about the right time. The primitive equation model tends to overshoot. In reality, much of the velocity contrast, for instance at the gravity current head, is probably concentrated in thin shear zones, which are subject to Kelvin-Helmholz instability. This will lead to turbulent entrainment which should act as an effective brake on the circulation. These effects are missing in our simulations because of the lack of vertical resolution and the use of a two-dimensional model. The finite difference grid, however, appears to be able to resolve most aspects of the semi-geostrophic solution adequately, as judged by comparison with the geometric model. The geometric model solutions suggest that neglect of cross-coastal friction is quite serious, the scale of the sea-breeze in the horizontal is expanded and the evening acceleration lost. The use of a different definition of balance which retains advection of the ageostrophic wind by the geostrophic flow, such as the nonlinear balance equation, might improve some aspects of the simulations, such as the behaviour at the coast itself. However, new limitations might appear instead. The distortion of the horizontal scale would probably not be affected.

The primitive equation model can describe all types of motion and thus rectify the distortions caused by the balance assumption. However,

the resolution of the model is no longer adequate to describe the more complex behaviour, and the results show as many unsatisfactory features as the balanced model. The main ones are the overshooting tendency, the production of extensive regions of up-gradient flow, and the strength of the internal wave response. All of these require more detailed study in the context of operational mesoscale models and more detailed study of the observations. The vertical resolution required to model this more complex response adequately may be an order of magnitude greater than that used here, and the turbulence model may also need considerable improvement.

ACKNOWLEDGMENTS

The author would like to thank Dr. G. Shutts and Dr. S. Garner for reviewing an earlier version of this paper, and Mr. M. Hatton for programming assistance.

REFERENCES

Atkinson, B.W. 1981

Mesoscale atmospheric circulations. Academic Press.

Bell, R.S. and Dickinson, A. 1987

The Meteorological Office operational numerical weather prediction system. Meteor. Office Sci. Paper no. 41, HMSO.

Chynoweth, S. 1987

The semi-geostrophic equations and the Legendre transform. Ph.D. thesis, Dept. Maths., Univ. of Reading, U.K.

Cullen, M.J.P. 1988

Implicit finite difference methods for modelling discontinuous atmospheric flows. *J. Comput. Phys.*, to appear.

Cullen, M.J.P., Norbury, J.,

Purser, R.J. and Shutts, G.J. 1987

Modelling the quasi-equilibrium dynamics of the atmosphere. *Q. J. R. Meteor. Soc.*,113, 735-757.

Haurwitz, B. 1947

Comments on the sea-breeze circulation. *J. Met.*, 4, 1-8.

Holt, M.W. 1987

Moist frontogenesis in the geometric model. U.K. Met. Off., Met. O 11 Tech. Note no. 248.

Hoskins, B.J. and Bretherton, F.P. 1972

Atmospheric frontogenesis models: Mathematical formulation and solution. *J. Atmos. Sci.*, 29, 11-37.

Houghton, D. 1984

Wind Strategy, Fernhurst Books, London.

Moura. A.D. 1976

The eigensolutions of linearized balance equations over a sphere. *J. Atmos. Sci.*, 33, 877-907.

Simpson, J.E. 1969

A comparison between laboratory and atmospheric density currents. *Q. J. R. Meteor. Soc.*, 103, 47-76.

Wu, R. and Blumen, W. 1982

An analysis of Ekman boundary layer dynamics incorporating the geostrophic momentum approximation. *J. Atmos. Sci.*, 39, 1774-1782.

Young, J.A. 1973

A theory for isallobaric air flow in the planetary boundary layer. *J. Atmos. Sci.*, 30, 1584-1592.

Yuen, C-W. and Young, J.A. 1986

Dynamical adjustment theory for boundary layer flow in cold surges. *J. Atmos. Sci.*, **43**, 3089-3108.

FIGURE CAPTIONS

Fig. 1 Initial element configuration for geometric model.

Fig. 2 Solutions after 12 hours with no basic state wind and total surface heating of 19°C. The coastline is in the centre of the cross-sections.

(a) Geometric model-element configuration.

(b) θ field, contour interval 0.5°C.

(c) Finite difference semi-geostrophic solution. θ field.

(d) v field, contour interval 1 ms^{-1}.

(e) u field, contour interval 0.5 ms^{-1}.

(f) Finite difference primitive equation solution, θ field.

(g) v field.

(h) u field.

Fig. 3 Cross-coastal wind component at 6 hour intervals for the experiment described in Fig. 2 using finite difference semi-geostrophic model. Contour interval 0.5 ms^{-1}. The coastline is in the centre of the cross-sections.

Fig. 4 As Fig. 3 using primitive equation model.

Fig. 5 Solutions after 12 hours with basic state wind of 5 ms^{-1} at 225° and heating of 19°C. layout of figure as Fig. 2. The coastline is in the centre of the cross-sections, except in

the geometric model simulations where it is as marked.

Fig. 6 As Fig. 5 with basic state wind direction 340° and heating of 7.5°C.

Fig. 7 As Fig. 5 with basic state wind direction 160° and heating of 7.5°C.

Fig. 8 As Fig. 5 with basic state wind direction 045° and heating of 19°C.

Fig. 1

1	7	13	19	25	31	37	43	49	55	61	67	73	79	85	91	97	103	109	115
2	8	14	20	26	32	38	44	50	56	62	68	74	80	86	92	98	104	110	116
3	9	15	21	27	33	39	45	51	57	63	69	75	81	87	93	99	105	111	117
4	10	16	22	28	34	40	46	52	58	64	70	76	82	88	94	100	106	112	118
5	11	17	23	29	35	41	47	53	59	65	71	77	83	89	95	101	107	113	119
6	12	18	24	30	36	42	48	54	60	66	72	78	84	90	96	102	108	114	120

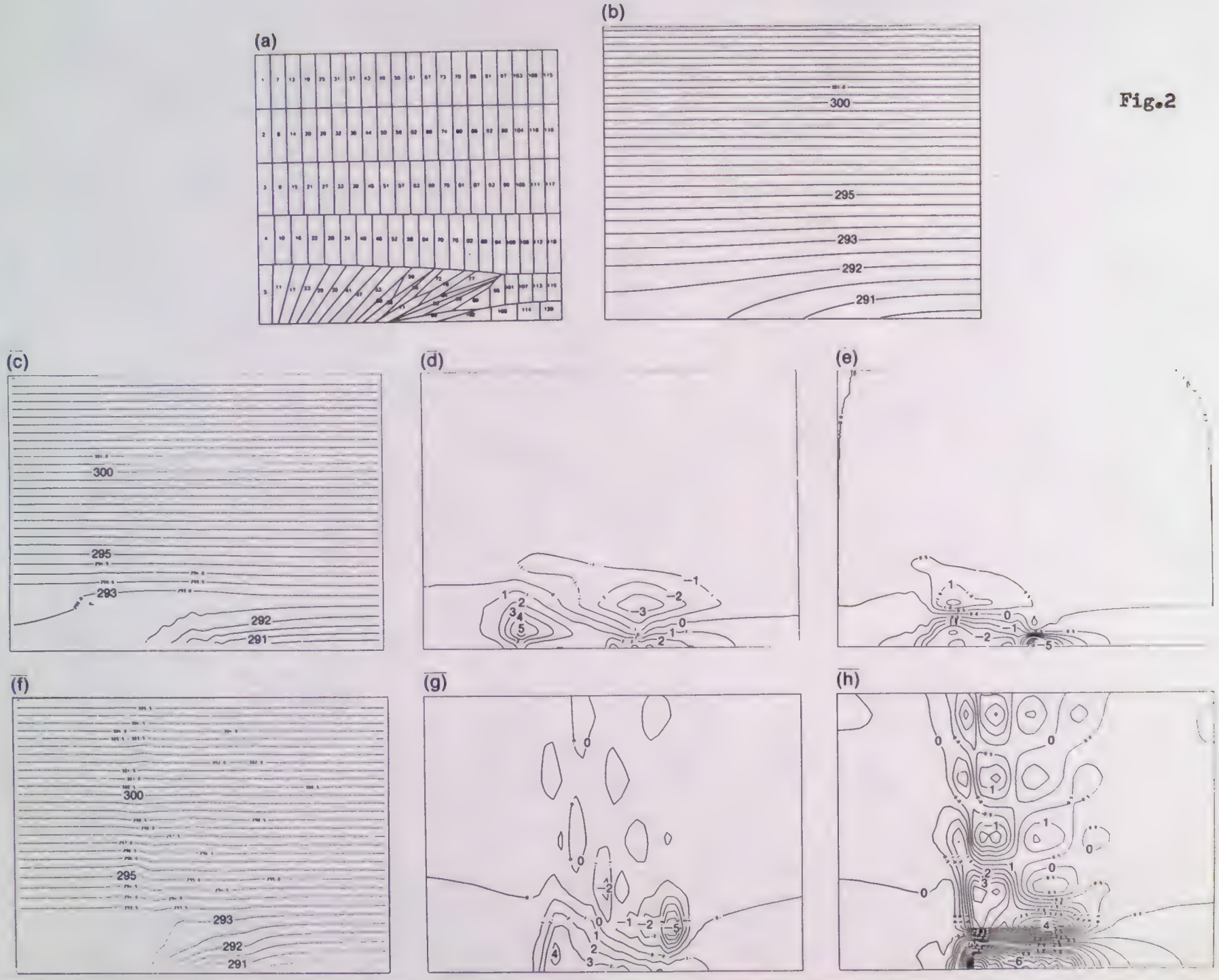
(a)
(b)
300
295
293
292
291
(c)
300
295
293
292
291
(d)
(e)
(f)
300
295
293
292
291
(g)
(h)

Fig.2

Fig. 3

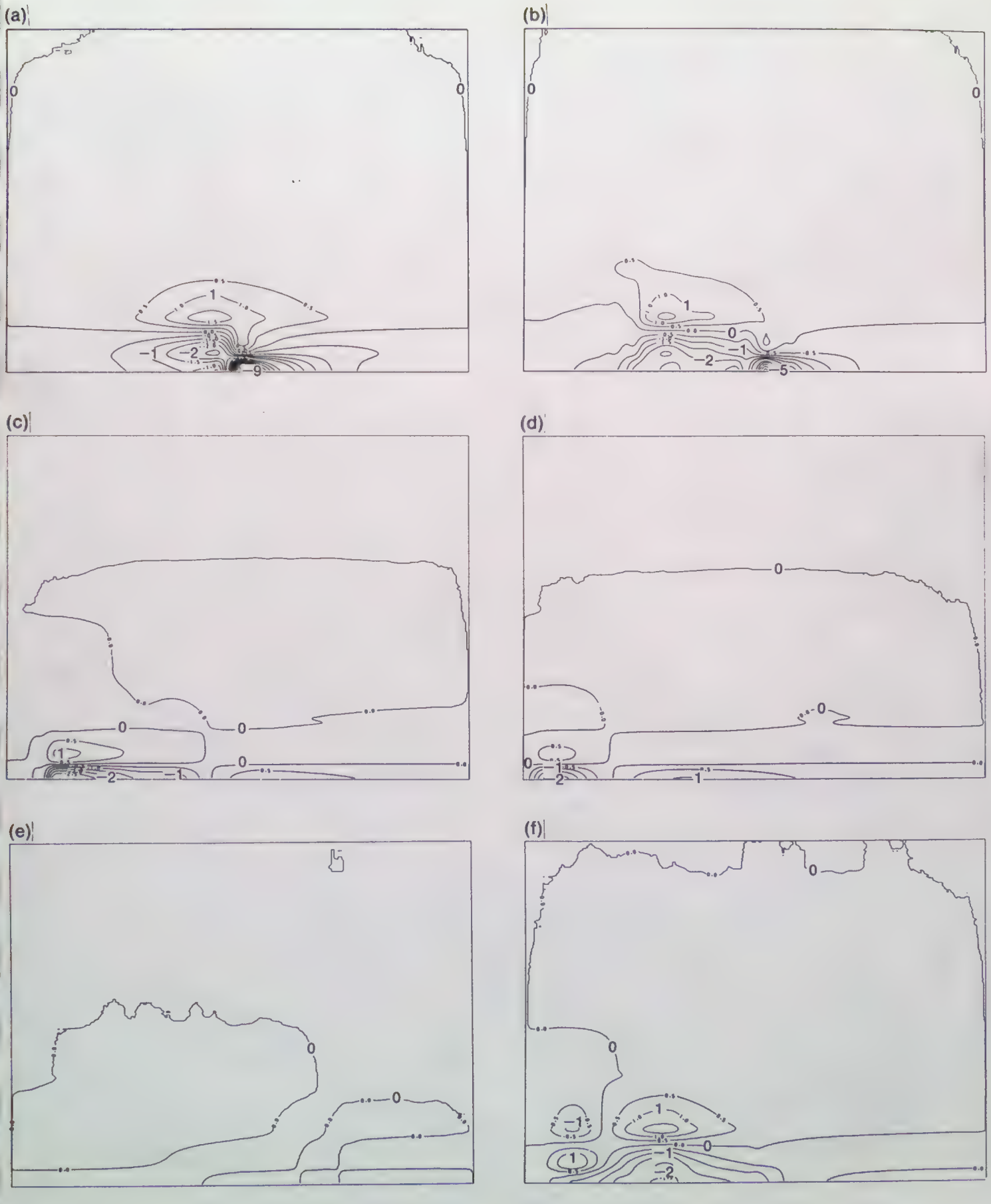

Fig. 4

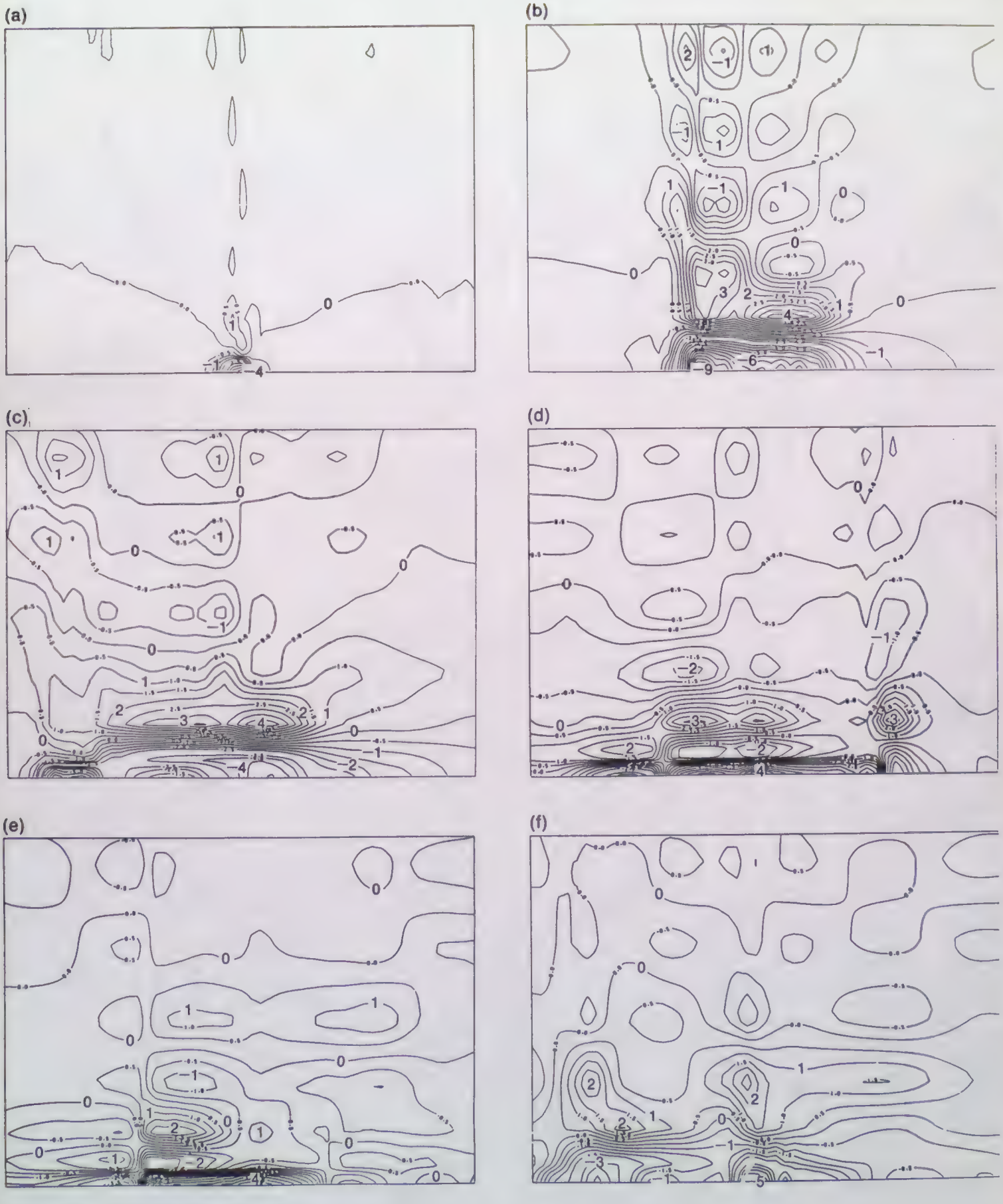

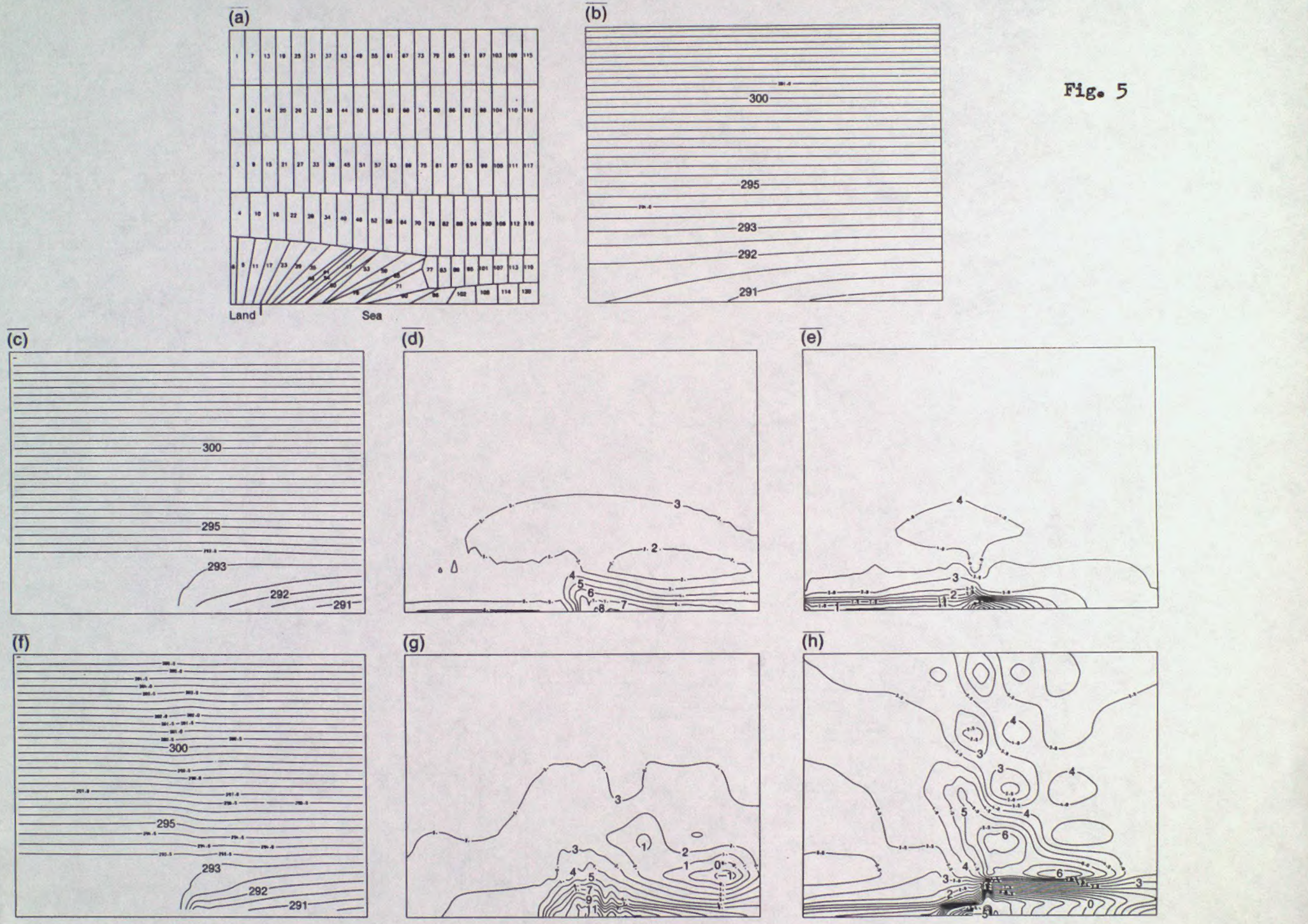
(a)
Land
Sea
(b)
300
295
293
292
291
(c)
300
295
293
292
291
(d)
3
2
4
5
6
7
8
(e)
4
3
2
1
(f)
300
295
293
292
291
(g)
3
1
2
0
(−1)
3
4
5
7
9
11
(h)
4
3
3
4
5
4
6
4
6
3
3
2
0
5

Fig. 5

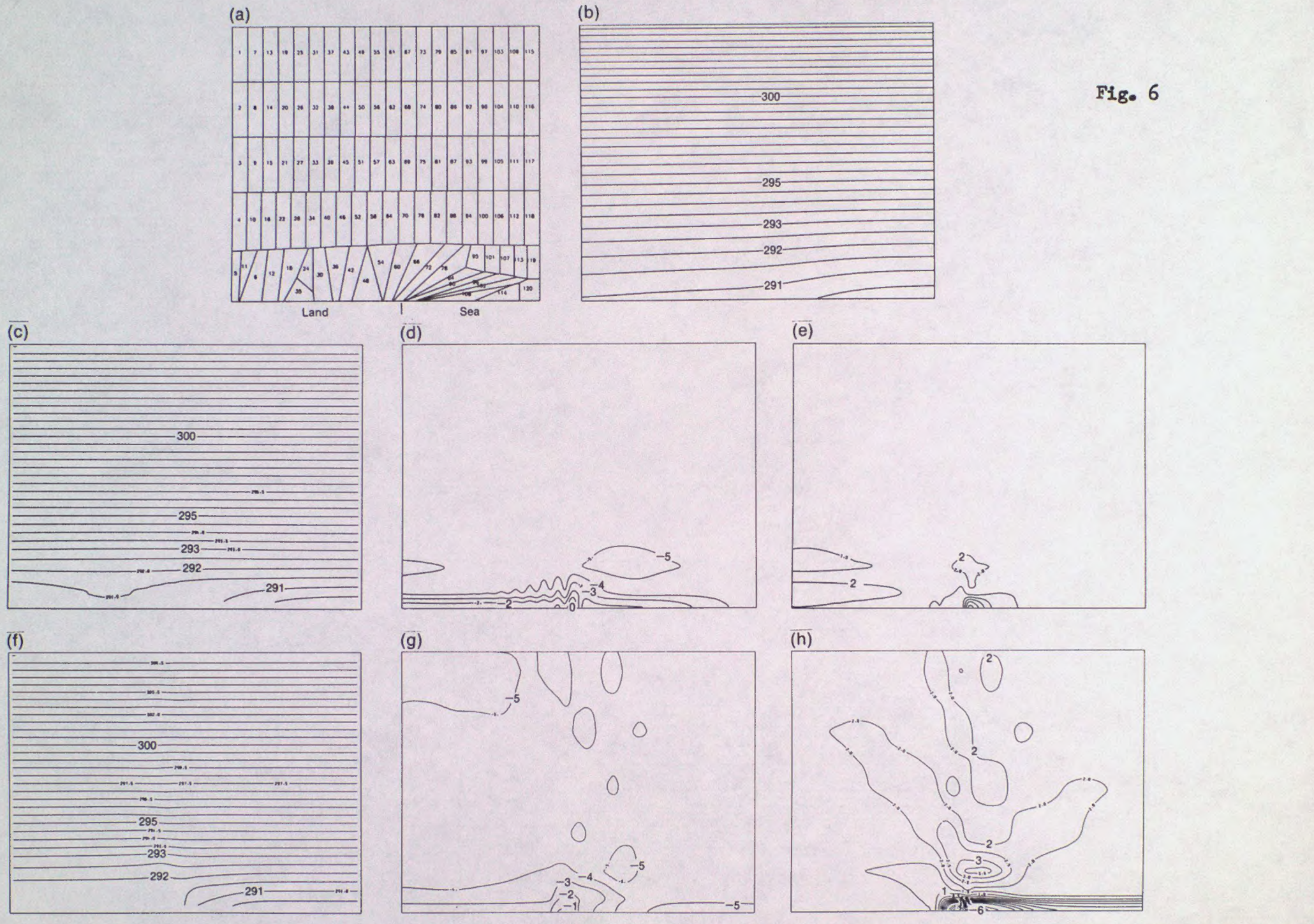
(a)
Land
Sea
(b)
300
295
293
292
291
(c)
300
295
293
292
291
(d)
-5
-4
-3
-2
0
(e)
2
2
(f)
300
295
293
292
291
(g)
-5
-5
-4
-3
-2
-1
-5
(h)
2
2
2
3
1
6

Fig. 6

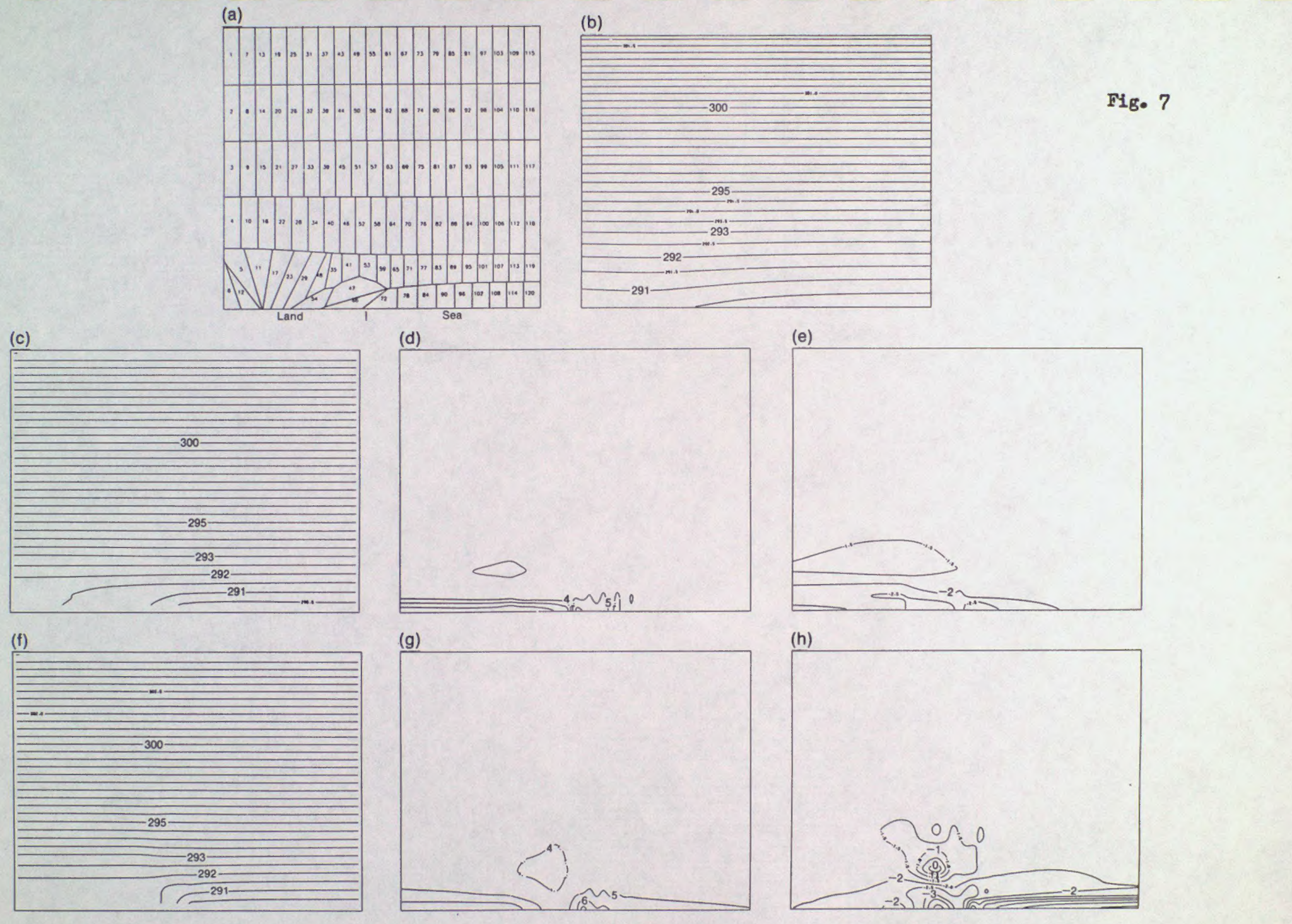
(a)
Land
Sea
(b)
300
295
293
292
291
(c)
300
295
293
292
291
(d)
4
5
(e)
-2
(f)
300
295
293
292
291
(g)
4
5
6
(h)
-1
0
-2
-3
-2
-2

Fig. 7

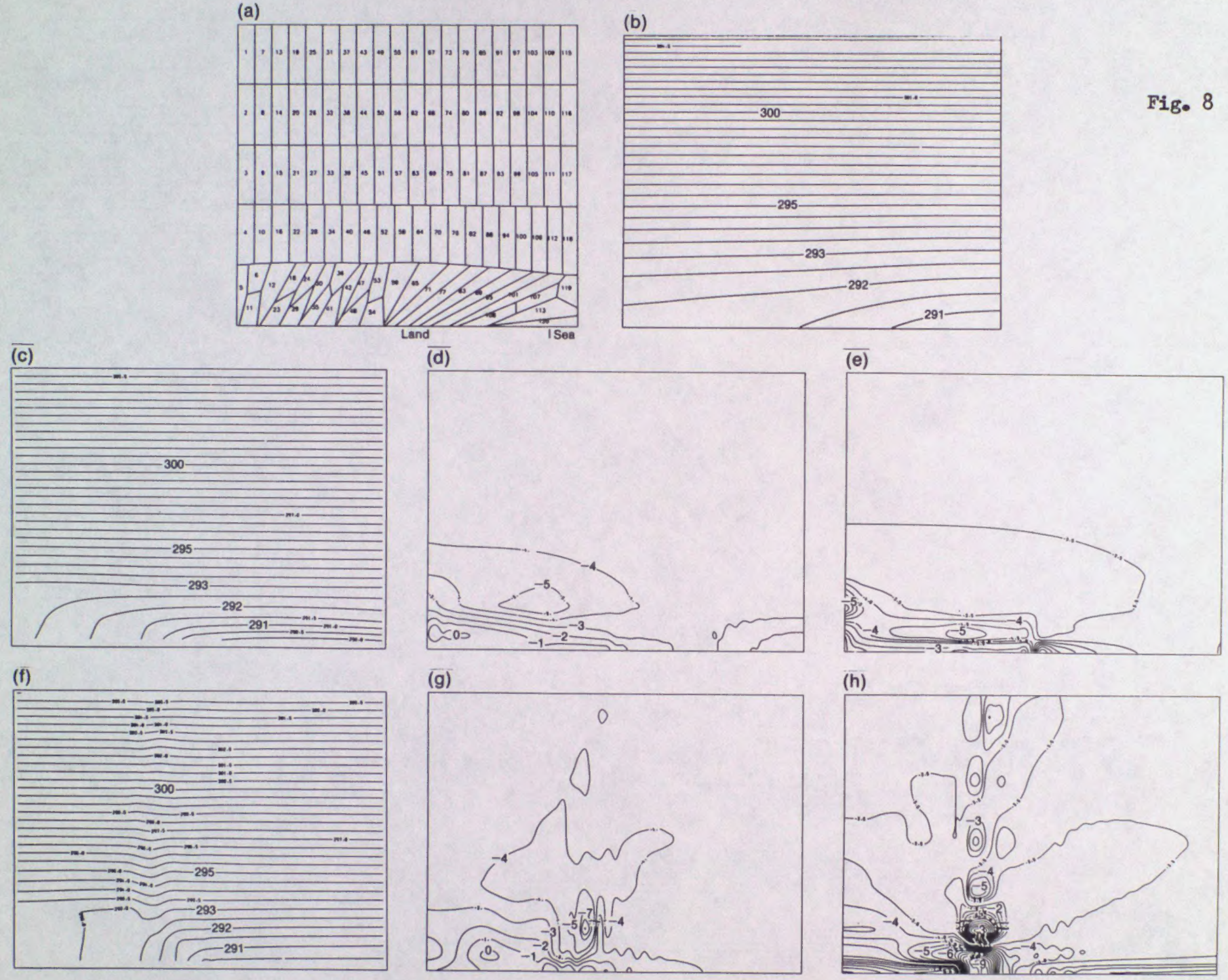
(a)
Land
Sea
(b)
300
295
293
292
291
(c)
300
295
293
292
291
(d)
(e)
(f)
300
295
293
292
291
(g)
(h)

Fig. 8